Journal of Phycology
April 2022, Volume 58, Issue 2, Pages 281-296
https://doi.org/10.1111/jpy.13232
https://archimer.ifremer.fr/doc/00743/85479/

Archimer
https://archimer.ifremer.fr

The possible fates of Fragilariopsis cylindrus (polar diatom) cells exposed to prolonged darkness

Sciandra Théo [1, 2], Forget Marie-hélène [1], Bruyant Flavienne [1], Béguin Marine [1], Lacour Thomas [3], Bowler Chris [2], Babin Marcel [1, *]

[1] Takuvik International Research Laboratory CNRS/Université Laval Département de Biologie Pavillon Alexandre-Vachon Québec QC, Canada
[2] Institut de Biologie de l'Ecole Normale Supérieure (IBENS) Ecole Normale Supérieure CNRS INSERM Université PSL 75005 Paris, France
[3] Ifremer, PBA, Rue de l'Ile d'Yeu BP21105, 44311 Nantes Cedex 03, France

* Corresponding author : Marcel Babin, email address : marcel.babin@takuvik.ulaval.ca

Abstract :

At high latitudes, the polar night poses a great challenge to photosynthetic organisms that must survive up to six months without light. Numerous studies have already shed light on the physiological changes involved in the acclimation of microalgae to prolonged darkness and subsequent re-illumination. However, these studies have never considered inter-individual variability because they have mainly been conducted with bulk measurements. On the other hand, such long periods are likely to impact within-population selection processes. In this study, we hypothesized that distinct subpopulations with specific traits may emerge during acclimation of a population of diatoms to darkness. We addressed this hypothesis using flow cytometry, which allow to individually characterize large numbers of cells. The ecologically dominant polar pennate diatom Fragilariopsis cylindrus was subjected to three dark acclimation experiments of one, three, and five months duration, during which all cultures showed signs of recovery once light became available again. Our results suggest that darkness survival of F. cylindrus relies on reduction of metabolic activity and consumption of carbon reserves. In addition, flow cytometry allowed us to record three different causes of death, each shared by significant numbers of individuals. The first rendered cells unable to survive the stress caused by the return to light, probably due to a lack of sufficient photoprotective defenses. The other two were observed in two subpopulations of cells whose physiological state deviated from the original population. The data suggest that starvation and failure to maintain dormancy were the cause of cell mortality in these two subpopulations.

Keywords : Flow cytometry, physiology, polar diatom, polar night, prolonged darkness, survival

Please note that this is an author-produced PDF of an article accepted for publication following peer review. The definitive publisher-authenticated version is available on the publisher Web site.

Abbreviations: DA, dark acclimation; DOC, dissolved organic carbon; FCM, flow cytometry; FSC, forward scatter; NL, neutral lipids; NPQ, non-photochemical quenching; P, population; RL, return to light.

This article is protected by copyright. All rights reserved

Accepted Article

INTRODUCTION

Rapid and strong abiotic environmental variations occurring in marine polar ecosystems pose a great challenge to microorganisms. At high latitudes, primary production (PP) is mainly generated by diatoms that often dominate blooms below the ice pack and in the water column when the snow and ice start to melt during spring (Von Quillfeldt 2000, Sakshaug 2004, Poulin et al. 2011). These cells typically experience an extreme light cycle over the year due to the high latitudes at the poles: summer is marked by a continuous light period of up to several months, while winter is characterized by an equally long dark period known as the polar night (up to six months; see Karsten et al. 2012, Cohen et al. 2020). In addition, light availability is drastically influenced by the dynamics of snow and sea ice, among other abiotic factors (e.g., Mundy et al. 2014). In this context, one essential question that remains unsolved is how diatoms, which spend extended periods deprived of any light source, manage to survive and start to proliferate again the following year.

Surviving without being able to perform photosynthesis means firstly being able to maintain metabolism via a durable alternative energy source. The alternative energy source could be intracellular or extracellular (dissolved organic carbon present in the surrounding environment). It has been proposed that diatoms could rely on three different strategies to survive darkness. The first is the consumption of cellular carbon reserves existing mainly as triacylglycerides (neutral lipids; NL) and chrysolaminarin (carbohydrates; Darley 1977, Biersmith and Benner 1998, Hu et al. 2008, Villanova et al. 2017). In addition, functional biomass (i.e., proteins, nucleic acids and structural lipids) was also observed to be consumed in the dark (Handa 1969, Anderson 1976, Schaub et al. 2017). The second strategy is the formation of resistant/dormant cells, the two forms known for diatoms being resting spores (or resting cysts) and resting cells (see McQuoid and Hobson 1996). Both are characterized by a reorganization of cytoplasmic material (Sicko-Goad et al. 1986, 1989, Pitcher 1990, du Preez et Bäte 1992), the function of which is yet to be understood, but spores differ from resting cells by the presence of thicker frustules, and sometimes the addition of siliceous spines on its surface **(**Pitcher 1990**,** Sugie et al. 2010**)**. While spores have already been reported during darkness acclimation (Smayda and Mitchell-Innes 1974), they are mostly observed during nutrient stresses (see McQuoid and Hobson 1996), unlike resting cells (Anderson 1976, Palmisano and Sullivan 1983, Sicko-Goad et al. 1989, du Preez and Bäte 1992). The third and last strategy is the use of secondary heterotrophy.

This article is protected by copyright. All rights reserved

Although diatoms are generally considered as obligate autotrophic organisms, it has long been known that some species can assimilate certain sources of organic carbon present in the surrounding environment (Lewin 1953, Hellbust and Lewin, 1977, Zhang et al. 1998). Bowler et al. (2008), in sequencing the genome of *Phaeodactylum tricornutum*, found that the complex evolutionary history of diatoms has resulted in them retaining some genes from a heterotrophic ancestor, and has also been punctuated by lateral transfers of bacterial genes that enable diatoms with heterotrophic potential. Traller et al. (2016) sequenced the nuclear genome of *Cyclotella cryptica*, a diatom capable of heterotrophic growth (see Pahl et al. 2010 and references therein) and revealed the presence of a wide range of sugar transporters. In 2017, Villanova et al. also showed in a light-grown strain of *P. tricornutum* that the addition of a dissolved organic carbon (DOC) source could drastically affect the management of its carbon metabolism, both at the physiological and molecular levels. In particular, the addition of glycerol to the culture medium led to an increase in the storage and consumption of lipids (TAG reserves in particular) and carbohydrates. More recently, studies have been conducted to improve industrial production processes of molecules of interest by using a DOC source such as glycerol to induce mixotrophic growth in diatom cultures (see Yang and Wei 2020 and references therein). These studies suggest that heterotrophy may, in addition to supporting basal metabolism in the dark, increase survival potential based on mobilization of reserves when they are built up prior to the complete disappearance of light.

Although some diatoms may actively grow on external sources of DOC, the very low cell concentrations observed in water and ice during the polar winter (Horner and Schrader 1982) suggest that most species do not possess a strong enough heterotrophic potential, or that the availability of DOC is not high enough to support significant growth. All of the three strategies mentioned above are likely accompanied by a cessation of growth as well as a significant slowing of metabolism. This would decrease the rate of consumption of available resources and increase survival time.

To be able to resume normal activity when light returns, it is necessary for cells to have been able to maintain the integrity of essential functions during darkness. Photosynthesis is obviously one of them. Preparation for resumption of growth therefore involves maintaining a viable photosynthetic apparatus as well as the ability to survive light stress. Various studies have shown that the chl *a* and ribulose-1,5-biphosphate carboxylase/oxygenase content of diatoms only decreases slightly during a

This article is protected by copyright. All rights reserved

Accepted Article

Accepted Article

period of prolonged darkness (Peters and Thomas 1996, Lacour et al. 2019). The same is true for diadinoxanthin and diatoxanthin contents (Lacour et al. 2019, Morin et al. 2019), which are responsible for generating a strong non-photochemical quenching (NPQ) during light stress (Lavaud et al. 2002). In addition to the maintenance of NPQ in darkness, other reported mechanisms that may help diatoms to successfully recover from long periods of darkness include the management of reactive oxygen species generated during reillumination, partial restructuring of PSII that can be rapidly reversed when light returns, maintenance of active ATP synthase mediated by chlororespiration, and possible alternative electron sinks to limit photodamage (Lacour et al. 2019 and references therein). Finally, it should be noted that cellular recovery likely has an energy cost that must be met by the resources available at the end of the dark period to rebuild what was lost/compromised during darkness (Peters and Thomas 1996).

While long term dark survival of polar (and temperate) microalgae has already been extensively studied (see Wulff et al. 2008 for review; Kamp et al. 2011, nitrate respiration in dark and anoxic conditions; Kennedy et al. 2019, respiration of lipids, carbohydrates and proteins; Kvernvik et al. 2018, maintenance of the activity of the photosynthetic machinery; Lacour et al. 2019, influence of light intensity on recovery after darkness and photosynthesis management; Martin et al. 2012 and Reeves et al. 2011, influence of temperature on dark survival and photosynthesis capacity; Morin et al. 2019, photosynthesis management; Schaub et al. 2017, influence of temperature on carbohydrate and lipid consumption; Veuger and Oevelen 2011, pigment degradation; Walter et al. 2017, influence of short light periods during darkness on survival), the mechanisms triggering each of these strategies as well as their relative importance remain however unclear. Studies are typically based on a rather narrow set of key physiological parameters (e.g., pigmentation, growth rate, cell size), and most, if not all, previous studies, with the exception of Naik and Anil (2018) which deals with *Tetraselmis indica* (chlorophyte) survival in darkness, have based their approach on classical physiological techniques used to obtain bulk values of measured properties, rather than single-cell properties. This can greatly limit the ability to understand survival strategies in the dark. Indeed, previous studies only provide access to the mean values of the parameters studied, whereas any change in growth conditions could trigger a spectrum of responses and physiological states within a population. The inability to take this

This article is protected by copyright. All rights reserved

inter-individual variability into account can significantly affect interpretation of the data, especially if part of the population loses viability during the treatment.

Here, we use single-cell data obtained by flow cytometry (FCM), combined with more conventional physiological methods, to better assess the different fates of a polar diatom during long term dark acclimation (DA) and subsequent re-illumination. FCM systems offer the advantage of being able to rapidly analyze a large number of cells (i.e., hundreds per second). They also benefit from the availability of numerous off-the-shelf fluorescent dyes that allow diverse physiological analyses to be performed, such as cell viability, cell cycle progression, apoptosis occurrence, reactive oxygen species detection, membrane potential, etc.

In this study, three long term acclimation experiments to total darkness of one, three, and five months were carried out on axenic batch cultures of the polar pennate diatom *Fragilariopsis cylindrus*. Each dark treatment was followed by up to three weeks re-acclimation to light. FCM measurements allowed us to follow the survival of *F. cylindrus* during each of these treatments and permitted us to identify different subpopulations during darkness. They were distinct from the initial population and experienced different fates following the return to light.

MATERIALS AND METHODS

Biological material

The experiments were conducted on a monoclonal axenic strain of *Fragilariopsis cylindrus* isolated from the strain CMMP1102 (National Center for Marine Algae and Microbiota, Bigelow, USA). This psychrophilic microalga is one of the dominant species regularly recorded at the poles, both within ice and in subsequent planktonic blooms (Kang and Fryxell 1992, Gleitz and Thomas 1993, Von Quilfeldt 2000).

Culture system and experimental planning

Before the experiments, *Fragilariopsis cylindrus* was cultivated in semi-continuous stable conditions in different vessels of incremental volumes that allowed to reach sufficient biomass required for the experiments (see details in Table S1 in the Supporting Information). For each of the three

This article is protected by copyright. All rights reserved

experiments, triplicates of cultures were cultivated in 80 L glass cylinders (diameter: 30 cm, height: 140 cm) that were placed in a cold room (0°C). *Fragilariopsis cylindrus* was grown in artificial seawater enriched with Aquil medium (Price et al. 1989). The culture medium was filtered successively on two polypropylene felt filter bags of 0.1 µm and 1 µm (Cole parmer, CAT# OF-01516-04 and CAT# OF-01516-20) and two pleated filter cartridges of 0.2 µm (GE Memtrex MP E filter, MMP921AAE-E; Cole parmer, FV- 06479-60) before it was sterilized with a UV lamp (Q30IL, Aquamerik, Saint-Nicolas, Quebec, Canada). Cultures were kept homogeneous through agitation with a magnetic stirrer. Temperature was maintained at 0 ± 1°C for the whole duration of the experiments. The cultures were bubbled with air successively filtered through a carbon filter (Carbon Cap 75, Whatman®) and an integral venting 0.2 µm filters (PolyVENT 500, Whatman®) to avoid limitation in dissolved inorganic carbon and dissolved oxygen. After a minimum of two weeks acclimation at 30 µmol photons · m^{-2} · s^{-1} in semi-continuous cultivation, triplicates of cultures growing exponentially were transferred to total darkness after they reached a cell concentration close to 1.0 x 10^6 cells · mL^{-1}. The cultures were submitted to DA of either one month (29 d), three months (88 d), or five months (145 d). At the end of each DA phase, cultures were re-exposed to the initial light conditions to follow the recovery of growth (return to light = RL). Experiments were terminated either three weeks after RL, or when the growth began to be nutrient-limited, whichever came first. The sampling frequency was high after the two light shifts and was progressively reduced as cell physiology stabilized over time (see Studied Parameters section). Overall, at least two samplings were conducted per week.

The lighting system consisted of a cardboard cylinder adapted to the shape of the cylindrical tanks. On the inside, evenly spaced LEDs generated cold white light that passed consecutively through five filters: a non-polarizing diffuser filter, three gelatin-colored filters (LEE filters, ref 138, 007, 137) and a 30%-transmittance neutral filter. The light spectrum can be found in Figure S1 in the Supporting Information. Ventilation systems were installed at the basis of the cylinders to evacuate the heat generated by the light system.

In acclimation experiments, control cultures are often monitored in parallel with cultures subjected to the treatment being studied to ensure that the observed responses are solely due to the treatment. For long periods of time such as those tested in this study (i.e., one to five months), cells exposed to constant light in a closed system would continue to grow until they quickly become

This article is protected by copyright. All rights reserved

limited by one or more nutrients. Therefore, the cultures would not only be compared based on the light conditions to which they are exposed, but also based on their different nutrient status. Another option would have been to regularly dilute cultures exposed to constant light with fresh media to maintain exponential cell growth (semi-continuous system). But this would also imply a difference in nutritional status. In addition, dilutions are known to sometimes temporarily disrupt the physiology of microalgae. Therefore, the control cultures in this study were considered inappropriate.

Studied parameters

Flow cytometry

Cell concentration and proxies for cell size, chlorophyll *a* (chl *a*) and neutral lipid contents (NL), viability, axenicity and DNA fluorescence were measured at least two times a week (see details in Table S2 in the Supporting Information) using a flow cytometer (Guava® easyCyteTM BGV HT, Millipore-Merck KGaA, Darmstadt, Germany, catalog No. 0500-4030) equipped with a blue laser (488 nm, 150 mW) for excitation of chl *a* and the different molecular probes. Fluorescence emissions were measured with red (695/50 nm) and green (512/18 nm) filters, for chl *a* and the different dyes, respectively. This implies that double staining with different dies could not be made. The stability of the cytometer readings was checked regularly by addition of calibration microbeads to every sample (Fluoresbrite® Polychromatic Red Microspheres 2.0 µm, catalog No. 19508-2, Polysciences Inc, Warrington, PA, USA). Prior to each measurement, dye solutions of various molecular probes and suspensions (see details below) containing calibration microbeads were prepared with salted filtered Milli-Q® water (S = 40; purification system Thermo Scientific Barnstead Nanopure). The dye working solutions were thawed at room temperature and a few microliters of each solution were transferred in a 2 mL Eppendorf microtube® safe lock containing water (see details below). The dye solutions were then cooled in ice prior to cell inoculation. The samples were prepared in flat bottom clear sterile 96-well microplates (ref: 655161, Greiner Bio-One International, Austria) placed on ice. The dye solutions were distributed in the microplates before 40 to 125 µL of culture were added to reach a cell concentration between 3.0 and 4.0 x 10^5 cells · mL^{-1} in 250 µL of sample. The samples were mixed gently with a pipette a first time after cell inoculation, and a second time before the analysis. All the staining protocols were performed in darkness. Prior to each series of measurements,

This article is protected by copyright. All rights reserved

the dye solutions were used as blanks and also served to check the cleanliness of the cytometer. Each measurement was performed in triplicate for each of the biological replicate (i.e., three cultures for each DA treatment) and a minimum of 5,000 events were counted. For contaminant detection we used SYBR Green (see protocol below), and 20,000 events were counted in order to increase the probability of detecting any contamination, but only one replicate was performed for each culture due to time constraints (see Fig. S2 for examples of cytograms from each of the four sample types described below). Data were analyzed with the Guava InCyte™ Software (version 3.1).

All equipment was either UV-sterilized or autoclaved prior to use, and sample handling was conducted under a laminar flow hood when necessary.

Cell concentration, cell size and chlorophyll a

Cell concentration, forward scattering (FSC, cell size proxy) and red fluorescence naturally emitted by chl *a* excited with blue light, were assessed without the addition of any dye.

Neutral lipids

To estimate the NL cell content, BODIPY® 505/515 (4,4-Difluoro-1,3,5,7-Tetramethyl-4-Bora-3a,4a-Diaza-s-Indacene; ThermoFisher, catalog No: D3921) was used. This type of BODIPY is a membrane permeant that can bind to NL. Upon binding NL, it emits a green fluorescence (em. 500/510 nm) when excited with blue light (max. ex. 488 nm). Some studies have shown that BODIPY® 505/515 has a particularly good affinity for cytoplasmic lipid droplets that mainly contains triacylglycerides (Rumin et al. 2015 and references therein). Measurement of BODIPY fluorescence thus allowed a semi-quantitative estimation of NL since the intensity of fluorescence is correlated with the amount of stained reserve lipids. The BODIPY commercial solution was dissolved in 99% anhydrous dimethyl sulfoxide (DMSO) in order to produce a stock solution of 500 µM. We used the final concentration determined as optimal by Morin (2017) whose Master's degree also focused on the survival of *Fragilariopsis cylindrus* in extended darkness. Working solutions of 1.5 mL were prepared by dissolving the stock solution 20-fold in 99% DMSO in 2 mL Eppendorf tubes® (final concentration 25.4 µM), and stored in darkness at -20°C. During the analysis, the volume of BODIPY working solution added into the dye solution was adjusted to reach a final concentration of 0.33 µM and 1.32%

This article is protected by copyright. All rights reserved

DMSO once mixed in the culture sample. Samples were stained during one hour in a styrofoam box filled with ice.

Viability

Within a highly concentrated culture, there is no simple way of knowing how many cells are either alive, dying, or already dead. Different proxies of viability are thus routinely utilized, including membrane permeability and enzymatic activity, sometimes combined together, in order to obtain more accurate results (Olsen et al. 2016). Because it was expected that metabolism would be dramatically diminished during long periods of DA, we decided to monitor viability by checking the membrane permeability of cells with SYTOX™ Green Nucleic Acid Stain - 5 mM Solution in DMSO (ThermoFisher, catalog No: S7020) (Peperzack and Brussaard 2011). When the cytoplasmic membrane is damaged and has lost its integrity, SYTOX Green can penetrate the cells and bind to the DNA. The latter then emits a green fluorescence (504/523 nm) when excited with blue light (max. ex. 588 nm), that allows to distinguish dead/dying cells from the viable ones. Viability is then expressed as the percentage of non-stained cells. The efficiency of the protocol was verified with mixtures of healthy and heat-treated cultures. Surprisingly, the protocol worked much better at room temperature (22°C). Keeping cells at high temperatures (i.e., compared to culture conditions) during the staining did not introduce a bias by affecting the viability of the samples. SYTOX Green working solutions were prepared by diluting the commercial solution one hundred-fold in 35% DMSO in Milli-Q water and were stored in the dark at -20°C. During the analysis, the volume of SYTOX Green working solution added to the dye solution was adjusted to reach a final concentration of 1 µM once mixed in the culture sample. Samples were stained for one hour at room temperature.

Axenicity control and DNA fluorescence

We monitored for possible bacterial contamination of cultures with SYBR™ Green I Nucleic Acid Gel Stain - 10,000X concentrate in DMSO (ThermoFisher, catalog No: S7563). SYBR Green is membrane permeant and stains nucleic acids once it has entered the bacterial (or microalgal) cells (with the following preferential affinity: double stranded DNA >> single stranded DNA > RNA). Once bound, it emits a green fluorescence (max. em. 520) when excited with blue light (max. ex. 497

This article is protected by copyright. All rights reserved

nm). This dye allows detection of organisms (usually bacteria) that may be mingled with the noise if they are too small or not characterized by any auto-fluorescence emission. SYBR Green working solutions were prepared by diluting the commercial solution one hundred-fold in 35% DMSO in Milli-Q water and stored in darkness at -20°C. During the experiments, the volume of SYBR Green working solution added to the dye solution was adjusted to reach a final concentration of 2X once mixed in the culture sample. Samples were stained for one hour in a styrofoam box filled with ice.

Measurement of other physiological parameters

The sampling frequency of the following parameters was the same as for FCM analysis (see details in Table S2 in the Supporting Information).

Cell concentration and cell size

Cell concentration and cell size (in µm) were also estimated in triplicates with a Beckman Multisizer 4e Coulter Counter (Beckam Coulter, Indianapolis, IN, USA) equipped with a 50 µM aperture tube. The culture aliquots were diluted in salted Milli-Q water (S = 36) 40 or 80 times depending on the cell concentration. The Coulter Counter was calibrated using 10 µm latex beads (COULTER CC Size Standard L10, REF: 6602796, Beckman Coulter).

Particulate carbon

Twenty milliliters of culture were filtered onto precombusted (450°C for 4 h) glass-fiber filters (Cytiva® GF/F, 25mm, 0.7 µm nominal porosity) before they were dried and kept desiccated until analysis. The cell carbon quota was estimated in triplicate with a CHN analyzer (2400 Series II CHNS⁄O; Perkin Elmer, Norwalk, CT, USA).

Pigment content

One aliquot of 10 mL was sampled for each culture and filtered on glass-fiber GF/F filters (0.7 µm, 25 mm, Whatman®) for pigment analysis. The filters, conserved in 2 mL polypropylene cryovials (internal thread cap), were flash frozen in liquid nitrogen and stored at -80°C. Chlorophylls *a* and *c*, β-carotenes, zeaxanthin, antheraxanthin, violaxanthin, fucoxanthin, diadinoxanthin and diatoxanthin

This article is protected by copyright. All rights reserved

contents per cell were estimated by high performance liquid chromatography (HPLC) according to Ras et al. (2008) using a Zorbax Eclipse XDB-C_8 3.5µm column (Agilent Technologies, Santa Clara, CA, USA).

Statistical methods

Statistical tests were conducted on R v. 3.6.2 (R Core Team 2021). In the following paragraph, packages to which functions belong are only mentioned if the functions are not included in the base-R package stats v. 3.6.2 (R Core Team 2019). Shapiro-Wilk test (function Shapiro.test()) showed that the data compared with statistical tests were not following a normal distribution. Significance of the differences between data collected at different time points was tested with a paired Wilcoxon's test (function wilcox.test()). When different populations of cells of a same CMF sample were compared, unpaired Wilcoxon's test was used. When time series of a parameter for different cell populations were compared, the test was applied to the values of the time point for which the average difference between populations was smallest. One-sided alternative hypotheses were mentioned when used. To test the significance of correlations between parameters, Spearman's correlation coefficient (ρ) were calculated with the associated p-value (function cor.test(method = "spearman")). The stationary character of time series have been tested with Kwiatkowski-Phillips-Schmidt-Shin test (kpss.test() from the package tseries v. 0.10-48; Trapletti and Hornik, 2020). Multimodality of cell size distributions was tested with Hartigans' Dip Test (function dip.test() of the package diptest v. 0.76-0; Maechler 2021). To test the significance of differences between treatments (i.e., DA length) a Kruskal-Wallis test was applied (function kruskal.test()). The significance level was set at 5% ($\alpha = 0.05$).

RESULTS

Influence of DA length and re-illumination on cell survival and recovery

In each of the three treatments the *Fragilariopsis cylindrus* cultures survived darkness and, following re-illumination, we were able to detect an increase in cell volume (data not shown) and concentration (see Table 1). The latency time prior to cell division increased with the darkness phase duration (p-

This article is protected by copyright. All rights reserved

value < 0.02), as already observed in previous studies (Peters 1996, Peters and Thomas 1996, Karsten et al. 2012, Naik and Anil 2018; see Table 1).

In darkness, cell viability decreased significantly in the 1 and 5-month DA treatments according to statistical tests (p-values: 0.004, 0.9, 0.002 for 1, 3 and 5 months, respectively, with viability at T0 "greater" than viability at day 87 of DA) but was only important in the latter. In the 5-month DA, the decrease began around day 30 and tended to accelerate exponentially over time (see Fig. S3 in the Supporting Information). Viability did not decrease significantly during the 3-month DA treatment. The proportion of cells dying during RL also increased with DA length, to the extent that the FCM data from the 5-month DA treatment were often too noisy due to large amounts of dead/dying cells. On the other hand, the one-month DA treatment was too short to see changes in cell populations that were observed over the course of the other experiments (3- and 5-month DA). We therefore chose to focus on the results of the 3-month DA treatment.

Carbon consumption

Overall, the NL content and carbon quota appeared to decrease continuously during DA (Fig. 1). The steeper decrease observed for these two parameters between the beginning of DA and day 3 results in part from some cells still dividing early in DA (see below). Indeed, when not normalized by cell concentration, the DOC data do not follow a significantly different trend during the first few days than the rest of the DA (data not shown, trend KPPS test p-value > 0.1).

Cells experience different fates

Cytometry data showed that two subpopulations, respectively named P2 and P3, that did not exist at the beginning of the darkness period, emerged from the initial population (P1) over time during DA (Fig. 2). P2 was characterized by its lower red fluorescence (chlorophyll) and FSC (size proxy) values, whereas P3 displayed a higher green fluorescence upon staining with SYBR Green. This section focuses mainly on what characterizes and distinguish P1, P2 and P3.

P1: Cells that survived darkness

This article is protected by copyright. All rights reserved

Between the beginning and the 6th day, cell concentration increased by 14.1 ± 9.2%, indicating that some cells continued to divide (Fig. 3; p-value < 0.005, with average cell concentration "greater" at T0). Nymark et al. (2013, and references therein) have previously reported that *Phaeodactylum tricornutum* cells complete an ongoing cell cycle when placed in the dark. Morin et al. (2019) and Lacour et al. (2019) made the same observation with *Fragilariopsis cylindrus* and *Chaetoceros neogracilis*, respectively. The total cell concentration then remained stable until the end of DA but after 30 d in the dark, the abundance of P1 cells began slowly to decrease while P2 and P3 populations began to emerge (Fig. 3).

Average FSC and chlorophyll fluorescence of the P1 population slowly decreased during DA, and then increased during the first 24 h of RL before they stabilized between 3 and 5 d post re-illumination (Fig. 4).

SYBR Green allows to stain and detect DNA. It was originally used to detect the possible presence of contaminating organisms, but because the DNA staining of *Fragilariopsis cylindrus* changed unexpectedly during the experiment, and followed an intriguing pattern (Fig. 5), we decided to include it in the analysis. The average green fluorescence of P1 decreased from 20,000 to less than 8,000 counts during the first 24 h of darkness. It then decreased at a lower rate before stabilizing at around 3,000 counts at around day 23 of DA. Afterward, it did not change significantly until RL (level KPSS test p-value = 0.08), when it began to increase and reached values similar to the initial ones after a few days (Fig. 5).

Note that because the different fluorescent probes used in this study are characterized by similar excitation and emission wavelengths, double staining was not possible. Moreover, it will be shown later that two of the populations identified as P3 could only be distinguished from P1 after being stained with SYBR Green fluorescence. Consequently, obtaining BODIPY fluorescence for only P1 or P3 populations was not possible.

P2: Population characterized by low red fluorescence, FSC and lipid content

After a few weeks, a distinct cloud of cells (denoted P2) began to appear on cytograms and grew exponentially ($\mu = 0.045 \cdot d^{-1}$; Fig. 3B, see Fig. S4 in the Supporting Information). This new subpopulation accounted for approximately 1% of the whole population after 31 d of DA, and for 9.31

This article is protected by copyright. All rights reserved

± 1.08% after 3 months of DA. Since the total cell concentration was stable during DA (Fig. 3A), we can conclude that the P2 (as well as P3) population was composed of cells derived from P1. Red fluorescence and FSC of P2 remained stable for the whole DA duration (Fig. 4; level KPSS test p-values for red fluorescence and FSC: 0.056 and > 0.1). Also, the values of these two parameters were significantly lower in P2 than in the P1 population (Fig. 4; p-values < 0.005 and < 0.01 for red fluorescence and FSC, respectively, with values of P1 "greater" than those of P2). Forward scatter is commonly used as a proxy for cell size. However, Coulter counter data suggested that these cells were not actually smaller than P1 cells, as we could not distinguish two size populations (see Fig. S5 in the Supporting Information; Hartigan Dip's test p-value for each culture: 0.91, 0.71, 0.49). Rather, because the average FSC was strongly correlated with the average red fluorescence and BODIPY fluorescence during DA (i.e., chl *a* and NL contents, see Fig. S6 in the Supporting Information; ρ for each culture at T0: 0.96, 0.95, 0.97; p-values < 0.001), we propose that the FSC signal was mainly driven by changes in the cellular content of dense material and related changes in the refractive index that modulate light scattering (e.g., Bricaud et al. 1988).

The viability of P2 cells estimated with SYTOX Green, although slightly lower than that of P1, remained high until the end of DA (above 90%, see Fig. S7A in the Supporting Information). However, a careful examination of the SYBR Green data revealed that the DNA of these cells was not properly stained because its average green fluorescence values were close to background levels (see Fig. S8 in the Supporting Information).

Before and during the whole DA, the shape of the cloud regrouping P1 and P3 indicates that the cells had a NL content proportional to their chl *a* content (Fig 6A; Spearman correlation coefficients for P1 at T0 and at the end of DA: 0.76 and 0.71; p-values < 0.001). This is not surprising considering that larger cells have, on average, higher chl *a* and carbon quotas. However, this relationship between the BODIPY fluorescence and chl *a* was much lower for P2 as data points were further spread apart and losing their collective "droplet" shape (Fig. 6A; Spearman correlation coefficients for P2 at the end of DA: 0.39; p-values < 0.001). Moreover, the mean BODIPY green fluorescence of P2 never varied in the dark (level KPSS test p-value > 0.1), was much lower than in P1 and P3 (p-value < 0.001 with P1 and fluorescence "greater" than P2 fluorescence), and was very similar to background noise (between 100 and 400 counts; Fig. 6B).

This article is protected by copyright. All rights reserved

During RL, the red fluorescence of P2 decreased rapidly (Fig. 4B) and the relationship between autofluorescence and FSC observed in healthy populations was partially lost (see Fig. S9 in the Supporting Information). Note that P2 cells were neither stained by SYTOX Green (see Fig. S7B) nor SYBR Green during RL. The cell concentration of P2 increased during the first days of RL because some cells from other populations (mostly P3 cells, see next section about P3) transitioned the same physiological state (i.e., low red fluorescence and FSC).

P3: A population with high SYBR Green fluorescence

Concomitant with the appearance of the P2 population, another population distinct from P1 appeared and grew exponentially ($\mu = 0.053 \cdot d^{-1}$) up to RL (Fig. 3B, see Fig. S10 in the Supporting Information). It accounted for more than 1% of the culture after 36 days of DA, and 16.71 ± 2.94% after three months. Cells belonging to P3 could be distinguished from the others by a much stronger SYBR Green staining (p-value < 0.005 with P3 fluorescence "greater" than P1 fluorescence) whose values were very close to those of P1 prior to darkness and a few days after RL (Fig. 5, see Fig. S10). Although lower on average, values of FSC and red fluorescence were very close to those of P1 (Fig. 4), to the extent that P3 could not be differentiated from P1 on cytograms based only on FSC or red fluorescence (Fig. S11 in the Supporting Information). Like for P2, these two parameters did not vary significantly during DA (level KPSS test p-values > 0.1). The decreases observed between day 36 and day 58 (Fig. 4) were probably due to some cells of P1 being counted as P3 cells. Indeed, two cells from P1 bound together can be counted as one event by the FCM. Such an event would be characterized by a very high SYBR Green fluorescence (parameter used to distinguish the two populations) and attributed to P3. Because the concentration of P3 was very low during this time, a small amount of P1 cells could markedly influence the red fluorescence and FSC averages. Such a bias is visible in the decrease of standard deviation between day 36 and 58 (Fig. 4). Because double staining was not an option, P3 could not be distinguished from P1 based only on SYTOX Green data. However, the viability of the population containing P1 and P3 was still close to 99% at the end of DA (data not shown), so we can assume that P3 cells were still healthy.

During RL, while P1 showed signs of recovery (increase in FSC, red fluorescence, and DNA fluorescence; Figs. 4 and 5) the FSC and red fluorescence of P3 rapidly decreased to low levels (Fig.

This article is protected by copyright. All rights reserved

4) and cells from P3 became progressively indistinguishable from P2 in terms of red fluorescence and FSC (see Fig. S12 in the Supporting Information). Finally, cell concentrations of P3 also decreased rapidly (Fig. 3B, see Fig. S13 in the Supporting Information). During the first three days of RL, before any growth could be observed and while P2 concentrations increased by $1.42 \pm 0.25 \times 10^5$ cells $\cdot$ mL^{-1}, P3 concentrations decreased by $1.35 \pm 0.18 \times 10^5$ cells $\cdot$ mL^{-1} (Fig. 3B).

DISCUSSION

The aim of this study was to assess the evolution of carbon and NL contents in *Fragilariopsis cylindrus* during DA, as well as to examine the fate of individual cells. Overall, the data suggest that *F. cylindrus* cells rely on metabolic downgrading and carbon consumption for dark survival. Moreover, flow cytometry offered valuable insights into the possible fates of *F. cylindrus* cells when they undergo long periods of darkness such as encountered during the polar night. It allowed us to identify distinct cell subpopulations, each characterized by different survival capabilities. Evidence is presented here for three potential physiological states that rendered some of the cells unable to recover upon re-illumination.

Metabolic slowdown and carbon consumption

The consumption of carbon reserves associated with a reduction of metabolism is thought to be one of the strategies on which diatoms could rely to survive prolonged darkness. Gleitz and Kirst (1991) showed that diatom-dominated assemblages could significantly increase their investment of newly fixed carbon in lipids when light exposure was severely reduced (from 81 or more to less than 20 µmol photons $\cdot$ m^{-2} $\cdot$ s^{-1}). Their results suggest that lipids may account for more than 30% of total fixed carbon and thus may be a major energy source for survival during the polar night. Like Morin et al. (2019) and Schaub et al. (2017), our results do indicate that consumption of reserve lipids is part of the survival strategy of diatoms exposed to prolonged darkness. However, in our experiments, the summer to winter transition was simulated by immediate transfer of cultures from constant light to total darkness. Therefore, cells did not benefit from a gradual decrease in light before the start of DA like in the natural environment or as in the study by Gleitz and Kirst (1991). Under non-limiting

This article is protected by copyright. All rights reserved

growth conditions, lipids for example make up only a small percentage (10%) of macromolecular dry weight of *Phaeodactylum tricornutum* cells, with less than 50% of it being found in TAGs (Remmers et al. 2018). This is supported by the results of Gleitz and Thomas (1993), Thomas and Gleiz (1993), Palmisano et al. (1988) and Tillman et al. (1989), who showed that in polar diatoms (both in the field and in cultures), the relative amount of photosynthetically assimilated carbon invested into lipids is between 5 and 20% when temperature is at or below 0°C. In contrast, low molecular weight metabolites (primarily free amino acids and monosaccharides) are almost systematically the compartment in which carbon is most invested, sometimes accounting for more than 50% of total fixed carbon. Fahl and Kattner (1993) showed that although TAGs may represent the most abundant lipid class in polar diatom cells in both water and ice communities, lipids do not, however, represent a large portion of the dry weight (less than 15% in ice assemblages, and less than 5% in pelagic communities).

Excluding the three first days of DA during which some cells were still dividing, the carbon quota decreased on average by 29.11 ± 6.15%. Given the observations reported above, a decrease in carbon quota as large as measured here probably exceeded the initial amount of storage lipids in *Fragilariopsis cylindrus* at the beginning of DA. This suggests that *F. cylindrus* may have consumed other types of carbon-rich molecules to fuel its metabolism, as reported by Handa (1969) in *Skeletonema costatum* during a 10-d DA. The potential of other carbon compartments should therefore be investigated in the future.

At the beginning of DA, the SYBR Green data revealed an unexpected two-step decrease (within 24 h and 3 weeks). While the last rounds of cell division in some cells within the first three days of DA may explain part of this decrease, it cannot account for all of it. The decrease in SYBR Green fluorescence could have resulted from a decrease in plasma membrane permeability that could slow the staining. However, extending the staining time from 30 min to 2 h made no difference. In addition, the efficiency of SYTOX Green and BODIPY staining were never affected. A wide variety of processes acting on DNA, RNA and proteins are known to be involved in the regulation of cellular activity (review be Talbert et al. 2019). Some of these, such as histone (de)acetylation and (de)methylation, can alter the DNA landscape by condensing or expanding chromatin to varying degrees. The most packed areas of the genome are known as heterochromatin whereas the least

Accepted Article

This article is protected by copyright. All rights reserved

packed are denoted euchromatin. Formation of densely packed heterochromatin is suspected to provide a rapid means of making DNA physically unavailable to the transcription machinery. During nucleosome packing, the minor groove in the DNA, where SYBR Green binds, tends to be compressed and curved (Alberts et al. 2002). As a consequence, it can be "*kinked or alternately shifted*", reducing its accessibility (Richmond and Davey 2003, Ong et al. 2007). We therefore propose that the observed changes in SYBR Green fluorescence in darkness (that were reversed rapidly upon re-illumination) are the indirect sign of a higher degree of DNA packaging that allows *F. cylindrus* to shut down non-essential functions and to lower metabolic activity (i.e., a decrease in the consumption rate of its reserves) in the dark. This would increase its survival time but, as a consequence, also prevent the fluorescent molecule from binding to large areas of the genome.

P1: Survival during darkness does not guarantee growth recovery following re-illumination

While surviving without any external source of energy is the first challenge met by microalgae during the polar night, they can only participate in the new production season if they also manage to recover growth when light is available again. According to the viability data, most cells survived a 3-month DA. However, some of them, showing signs of degradation before and during RL (for P2 and P3, respectively), did not recover during RL. These cells were dead or virtually dead (i.e., unable to recover activity). This partly explains the significant decrease in viability observed during RL (-28.2 ± 4.1% after three days). In addition to cell death within the P2 and P3 populations, 20.7 ± 4.7% of the cells were no longer detectable after three days (day at which the viability reached a minimum). Assuming that all P2 and P3 cells died, and knowing their concentrations before RL, we can deduce that P2 and P3 populations represented 21.0 ± 1.8% and 37.8 ± 6.9% of the total cells that died during RL, respectively. Therefore, the remaining 41.2 ± 8.0% of the dead cells (or approximately 18% of all cells) died as a result of light stress. Because no cells died after one-month of DA we can conclude that this percentage increases with the length of DA, indicating that the cells weaken over time in darkness. The size of the remaining carbon pools may be of great importance during prolonged DA as it may help the cells to withstand light stress and rebuild what is necessary (i.e., pigment content, consumed and recycled material) to fully and quickly recover when light becomes available. However, NL content and carbon quota data showed a constant decrease during DA. Conversely, red

This article is protected by copyright. All rights reserved

fluorescence and HPLC dosages of pigments showed that the amounts of chl *a* and *c*, β-carotenes, fucoxanthin and diadinoxanthin linearly decreased during DA (the total amount of these pigments decreased by 28.9 ± 10.4% between day 3 and the end of DA, see Fig. S14 in the Supporting Information). The loss of pigments involved in photoprotection could have led to a decrease in photoprotective defenses over time, making them less likely to survive RL.

P2: Neutral lipid depletion and metabolic reduction

Cells belonging to P2 formed a population characterized by lower red fluorescence and NL content that grew exponentially following four weeks of darkness. They remained in a stable state until RL, after which they did not survive or show any sign of activity, their content being promptly degraded or released in the medium. The temporary increases of both P2 FSC and BODIPY fluorescence were probably the consequence of other cells (i.e., cells from P1 and P3) dying and entering the P2 physiological state. Indeed, while the concentration of P1 and P3 decreased, that of P2 increased.

The low and stable values of red fluorescence may reflect a partial degradation of chlorophyll to primary degradation products occurring when the cells enter the P2 state. These degradation products, such as pheophytin, may require photo-oxidation to further degrade to non-fluorescent metabolites, as observed during RL. During DA, SYBR Green seemed to be unable to stain these cells, indicating that the nucleic acid within P2 cells was probably degraded. If the DNA could not be stained by SYBR Green, it also means that the viability estimates obtained by SYTOX Green, which suggested that P2 was mostly viable, were actually not reliable for this population. During RL, the cells remained unstained with SYTOX Green or SYBR Green, confirming that they lost their DNA. We therefore consider that these cells were likely to be dead.

BODIPY measurements showed that the green fluorescence emitted by cells belonging to the P2 population was probably not generated upon binding with NL. Instead, we can assume that green fluorescence was generated by the presence of non-bound dye (see Rumin et al. 2015 and references therein). Govender et al. (2012) showed that, while concentrations of BODIPY 505/515 of 0.058 and 0.067 $\mu g \cdot mL^{-1}$ resulted in insufficient and optimal staining of NL in *Chlorella vulgaris*, respectively, a concentration of 0.083 $\mu g \cdot mL^{-1}$ was too high and generated a “bright background fluorescence”

This article is protected by copyright. All rights reserved

that hindered data collection. The concentration used in the present study was close to 0.082 µg · mL^{-1}. In the end, P2 cells appeared to be devoid of NL.

Collectively, all these elements suggest that these cells died during darkness. As *Fragilariopsis cylindrus* slowly consumed its NL content during DA, one possible limitation to its survival would be the size of its initial NL pool. Cells belonging to P2 could have died due to a depletion of their NL and could represent the fate of cells that exceeded their survival capacities. Interestingly, at the beginning of the 5-month DA, the mean NL content of the cells was only around 60% of the values obtained in the 3-month DA (mean green fluorescence value before darkness: 1206.26 ± 215.56 vs 2043.50 ± 215.56; p-value < 0.001 with 3-month DA values "greater" than 5-month DA values). The average carbon quota at T0 was also lower and represented around 84% that of the 3-month DA cultures (mean carbon quota value before darkness: $5.89 \times 10^{-6} \pm 6.97 \times 10^{-7}$ vs $7.02 \times 10^{-6} \pm 5.04 \times 10^{-7}$ µg C · $cell^{-1}$; p-value < 0.001 with 3-month DA values "greater" than 5-month DA values). If *F. cylindrus* does indeed rely on its NL content to survive darkness, this could explain why the cultures seemed to have a lower survival success during the 5-month DA, as they started to die after one month of darkness according to the viability data (see Table 1 and Fig. S3).

P3: Sleepwalker cells

Like P2 cells, the P3 population started to appear and to become more apparent following a couple weeks of darkness. But unlike P2, they were very similar to P1 in which they were evenly distributed and could not be distinguished on the basis of FSC, red fluorescence or NL content. They could only be identified based on higher SYBR Green fluorescence.

In some organisms, the increase of DNA fluorescence upon SYBR Green staining could be explained by a duplication of the genome that can offer different advantages to a cell such as an increased metabolic activity (Frawley et Orr-Weaver 2015). But even though observations of polyploid diatom cells have been made in the past (see von Dassow et al. 2008 and references therein, Mann 1994, Koester et al. 2010, van Tol et al. 2017), there is no solid evidence that diatoms are actually capable of endoreduplication (Huysman et al. 2014). The decrease in SYBR Green fluorescence observed in P1 at the beginning of DA can therefore be interpreted as a consequence of metabolic reduction. The finding that SYBR Green values of P3 were very close to those observed in

This article is protected by copyright. All rights reserved

active cells before DA could illustrate a change in chromatin structure synonymous with reactivation of cellular activity. P3 may be composed of cells whose dormancy system failed and led cells to death as they were not able to recover during RL.

During RL, FSC and red fluorescence of P3 cells decreased very rapidly to reach values similar to those of P2. While the concentration of P3 was dramatically decreasing (before they completely disappeared), the P2 population was increasing. This suggests that during RL, P3 lost their DNA and could not be detected on this criterion anymore, becoming therefore indistinguishable from P2. On the basis of Figure S13 it could be argued that we cannot be sure whether or not the population identified as P3 was really composed of cells from P3, and whether P3 cells were really converted to P2 cells. But the relative positions of these clouds during RL (see Fig. S13), the variations of their parameters (Fig. 4), as well as their respective cell concentrations (Fig 3B), suggest that the blue cloud (see Fig. S13) was indeed P3 and that cells belonging to this population all died and entered into a state similar to that of P2. In support of this, it should be noted that at the end of the darkness period of the 5-month DA experiment, when P3 and P2 represented a large majority of the cells in all cultures (data not shown), only 8% of the cells survived in the culture in which cell survival rate was the highest, indicating that a vast majority of the cells did not survive.

Finally, one might consider that P3 cells in darkness could be an intermediate state of P2 cells. At the end of the 5-month DA, most of the cells belonged to P2 or P3 (data not shown). If the above hypothesis was verified, we probably should have seen the P3 concentration decrease to P2 before the end of DA, which did not happen. While more evidence is needed, P2 and P3 therefore do not appear to be related.

In the present study, microscopic observations did not visually reveal the presence of any resting cells or spores. During acclimation experiments mimicking summer to winter transitions, Palmisano and Sullivan (1982) measured an increase of the heterotrophic potential of *Fragilariopsis cylindrus*. The ability of *F. cylindrus* to use heterotrophy is also suggested by transcriptome data of Mock et al. (2017). In the present study, however, no source of DOC was added to the culture medium and so heterotrophy was presumably not an option. Instead, our results suggest that *F. cylindrus* relies on a lowered metabolism combined with low consumption of neutral lipid reserves

This article is protected by copyright. All rights reserved

(and potentially other carbon pools), the depletion of which ultimately condemns the cells that were no longer stained by BODIPY. A biochemical analysis of the main carbon reservoirs, and in particular triacylglycerides, would be necessary to support this hypothesis. The fate of P3 cells is more obscure.

It should also be kept in mind that the strain studied was isolated over 40 y ago. It was deposited in the NCMA culture collection in 1982 by G. Fryxell. It has been cryopreserved since 2007 but has likely been in culture since then, so it is possible that it has drifted genetically from the original strain and is no longer representative of individuals found in their natural habitat. Despite this caveat, the choice was made to study this strain because it is the only polar diatom whose genome has been sequenced (Mock et al. 2017).

Flow cytometry has been instrumental for allowing the single cell approach reported here, and combining the information from different fluorescent probes has proven to be extremely useful. In the future, FCM could be an even more valuable tool as some cytometers are equipped to sort cells. Isolating different populations in order to observe them separately with different microscopic devices, for instance, could help us better understand the precise changes that occur in the different populations observed as well as the different cellular parameters on which selection pressure is exerted during the polar night.

ACKNOWLEDGMENTS

We thank Dominique Marie and Marianne Potvin for their help with flow cytometry protocols, Martine Lizotte for her valuable insights on interpretation of the results, Thomas Mock for providing the axenic strain of *Fragilariopsis cylindrus*, and all the Takuvik members who participated in the experiments. The Green Life in the Dark project was supported by the Human Frontier Science Program grant #RGP0003/2016 to MB and CB, Canada Excellence Research Chair on remote sensing of Canada's new Arctic frontier, Discovery grant #RGPIN-2020-06384 to MB, ArcticNet and the Sentinel North program of Université Laval, made possible, in part, thanks to funding from the Canada First Research Excellence Fund. Théo Sciandra was supported by Québec Océan and the FRQNT to conduct training program in Bigelow.

This article is protected by copyright. All rights reserved

Accepted Article

REFERENCES

Alberts, B., Johnson, A., Lewis, J., Raff, M., Roberts, K. & Walter, P. 2002. Chromosomal DNA and its packaging in the chromatin fiber. [Eds.] *Molecular Biology of the Cell*. 4th ed. Garland science, New York. USA, pp. 198–216.

Biernacki, C., Celeux, G. & Govaert, G. 2000. Assessing a mixture model for clustering with the integrated completed likelihood. *IEEE T. Pattern Anal.* 22:719–25.

Biersmith, A. & Benner, R. 1998. Carbohydrates in phytoplankton and freshly produced dissolved organic matter. *Mar. Chem.* 63:131–44.

Bricaud, A., Bédhomme, A. L. & Morel, A. 1988. Optical properties of diverse phytoplanktonic species: experimental results and theoretical interpretation. *J. Plankton Res*. 10:851–73.

Cohen, J. H., Berge, J., Moline, M. A., Johnsen, G. & Zolich, A. P. 2020. Light in the polar night. *In* Berge J., Johnsen G., & Cohen J. H. [Eds.] *POLAR NIGHT Marine Ecology*. Springer, Cham, Switzerland, pp. 37–66.

Darley, W. M. 1977. Biochemical composition. *In* Werner, D. [Ed.] *The biology of diatoms*. Blackwell. Oxford, UK. pp. 198–223.

von Dassow, P., Petersen, T. W., Chepurnov, V. A. & Virginia Armbrust, E. 2008. Inter-and intraspecific relationships between nuclear DNA content and cell size in selected members of the centric diatom genus *Thalassiosira* (Bacillariophyceae). *J. Phycol*. 44:335–49.

Fahl, K. & Kattner, G. 1993. Lipid content and fatty acid composition of algal communities in sea-ice and water from the Weddell Sea (Antarctica). *Polar Biol.* 13:405-9.

This article is protected by copyright. All rights reserved

Gleitz, M. & Kirst, G.O. 1991. Photosynthesis-irradiance relationships and carbon metabolism of different ice algal assemblages collected from Weddell Sea pack ice during austral spring (EPOS 1). *Polar Biol.* 11:385-92.

Gleitz, M. & Thomas, D.N. 1993. Variation in phytoplankton standing stock, chemical composition and physiology during sea-ice formation in the southeastern Weddell Sea, Antarctica. *J. Exp. Mar. Biol. Ecol.* 173:211-30.

Frawley, L. E. & Orr-Weaver, T. L. 2015. Polyploidy. *Curr. Biol.* 25:R353–R358.

Govender, T., Ramanna, L., Rawat, I. & Bux, F. 2012. BODIPY staining, an alternative to the Nile Red fluorescence method for the evaluation of intracellular lipids in microalgae. *Bioresource Technol*. 114:507–11.

Handa N. 1969. Carbohydrate metabolism in the marine diatom *Skeletonema costatum*. *Mar. Biol.* 4:208–14.

Hu, Q., Sommerfeld, M., Jarvis, E., Ghirardi, M., Posewitz, M., Seibert, M. & Darzins, A. 2008. Microalgal triacylglycerols as feedstocks for biofuel production: perspectives and advances. *Plant J*. 54:621–39.

Huysman, M. J., Martens, C., Vyverman, W. & de Veylder, L. 2014. Protein degradation during the diatom cell cycle: annotation and transcriptional analysis of SCF and APC/C ubiquitin ligase genes in *Phaeodactylum tricornutum*. *Mar. Genom*. 14:39–46.

Kamp, A., de Beer, D., Nitsch, J. L., Lavik, G. & Stief, P. 2011. Diatoms respire nitrate to survive dark and anoxic conditions. *Proc. Natl. Acad. Sci. USA* 108:5649–54.

This article is protected by copyright. All rights reserved

Kang, S. H. & Fryxell, G. A. 1992. *Fragilariopsis cylindrus* (Grunow) Krieger: the most abundant diatom in water column assemblages of Antarctic marginal ice-edge zones. *Polar Biol*. 12:609–27.

Karsten, U., Schlie, C., Woelfel, J. & Becker, B. 2012. Benthic diatoms in Arctic seas-ecological functions and adaptions. *Polarforschung* 81:77–84.

Kennedy, F., Martin, A., Bowman, J. P., Wilson, R. & McMinn, A. 2019. Dark metabolism: a molecular insight into how the Antarctic sea-ice diatom *Fragilariopsis cylindrus* survives long-term darkness. *New Phytol*. 223:675–91.

Koester, J. A., Swalwell, J. E., von Dassow, P. & Armbrust, E.V. 2010. Genome size differentiates co-occurring populations of the planktonic diatom *Ditylum brightwellii* (Bacillariophyta). *BMC Evol. Biol.* 10:1.

Kvernvik, A. C., Hoppe, C. J. M., Lawrenz, E., Prášil, O., Greenacre, M., Wiktor, J. M. & Leu, E. 2018. Fast reactivation of photosynthesis in Arctic phytoplankton during the polar night. *J. Phycol*. 54:461–70.

Lacour, T., Morin, P. I., Sciandra, T., Donaher, N., Campbell, D. A., Ferland, J. & Babin, M. 2019. Decoupling light harvesting, electron transport and carbon fixation during prolonged darkness supports rapid recovery upon re–illumination in the Arctic diatom *Chaetoceros neogracilis*. *Polar Biol*. 42:1787–99.

Lupette, J., Jaussaud, A., Seddiki, K., Morabito, C., Brugière, S., Schaller, H. & Maréchal, E. 2019. The architecture of lipid droplets in the diatom *Phaeodactylum tricornutum*. *Algal Res.* 38: 101415.

Mann, D. G. 1994. Auxospore formation, reproductive plasticity & cell structure in *Navicula ulvacea* and the resurrection of the genus *Dickieia* (Bacillariophyta). *Eur. J. Phycol*. 29:141–57.

This article is protected by copyright. All rights reserved

Martin, A., McMinn, A., Heath, M. Hegseth, E. N. & Ryan, K. G. 2012. The physiological response to increased temperature in over-wintering sea ice algae and phytoplankton in McMurdo sound, Antarctica and Tromsø sound, Norway. *J. Exp. Mar. Biol. Ecol*. 428:57–66.

McQuoid, M. R. & Hobson, L. A. 1996. Diatom resting stages. *J. Phycol.* 32:889–902.

Mock, T., Otillar, R. P., Strauss, J., McMullan, M., Paajanen, P., Schmutz, J., Salamov, A., Sanges, R., Toseland, A., Ward, B. J., Allen, A. E., Dupont, C. L., Frickenhaus, S., Maumus, F., Veluchamy, A., Wu, T., Barry, K. W., Falciatore, A., Ferrante, M. I., Fortunato, A. E., Glöckner, G., Gruber, A., Hipkin, R., Janech, M. G., Kroth, P. G., Leese, F., Lindquist, E. A., Lyon, B. R., Martin, J., Mayer, C., Parker, M., Quesneville, H., Raymond, J. A., Uhlig, C., Valas, R. E., Valentin, K. U., Worden, A. Z., Armbrust, E. V., Clark, M. D., Bowler, C., Green, B. R., Moulton, V., van Oosterhout, C. & Grigoriev, I. V. 2017. Evolutionary genomics of the cold- adapted diatom *Fragilariopsis cylindrus*. *Nature* 541:536–40.

Morin, P. I. 2017. Acclimatation à la nuit polaire puis au retour de la lumière chez la diatomée arctique *Fragilariopsis cylindrus*. Master dissertation, Université Laval, Québec, 61 pp.

Morin, P. I., Lacour, T., Grondin, P. L., Bruyant, F., Ferland, J., Forget, M. H., Massicotte, Donaher, N., Campbell, D. A., Lavaud, J. & Babin, M. 2019. Response of the sea-ice diatom *Fragilariopsis cylindrus* to simulated polar night darkness and return to light. *Limnol. Oceanogr.* 65:1041–60.

Mundy, C. J., Gosselin, M., Gratton, Y., Brown, K., Galindo, V., Campbell, K., Levasseur, M., Barber, D., Papakyriakou, T. & Bélanger, S. 2014. Role of environmental factors on phytoplankton bloom initiation under landfast sea ice in resolute passage, Canada. *Mar. Ecol. Prog. Ser*. 497:39–49.

Naik, S. M. & Anil, A. C. 2018. Survival in the dark: strategies adopted by *Tetraselmis indica* (Chlorodendrophyceae, Chlorophyta). *Mar. Biol. Res*. 14:448–53.

This article is protected by copyright. All rights reserved

Accepted Article

Nymark, M., Valle, K. C., Hancke, K., Winge, P., Andresen, K., Johnsen, G., Bones, A. M. & Brembu, T. 2013. Molecular and photosynthetic responses to prolonged darkness and subsequent acclimation to re-illumination in the diatom *Phaeodactylum tricornutum*. *PLoS ONE* 8:e58722.

Olsen, R. O., Hess-Erga, O. K., Larsen, A., Hoffmann, F., Thuestad, G. & Hoell, I. A. 2016. Dual staining with CFDA-AM and SYTOX Blue in flow cytometry analysis of UV-irradiated *Tetraselmis suecica* to evaluate vitality. *Aquat. Biol*. 25:39–52.

Ong, M. S., Richmond, T. J. & Davey, C. A. 2007. DNA stretching and extreme kinking in the nucleosome core. *J. Mol. Biol*. 368:1067–74.

Pahl, S.L., Lewis, D.M., Chen, F. & King, K.D. 2010. Heterotrophic growth and nutritional aspects of the diatom *Cyclotella cryptica* (Bacillariophyceae): Effect of some environmental factors. *J. Biosci. Bioeng.* 109:235-9.

Palmisano, A. C. & Sullivan, C. W. 1982. Physiology of sea ice diatoms. I. Response of three polar diatoms to a simulated summer-winter transition. *J. Phycol*. 18:489–98.

Palmisano, A.C., Lizotte, M.P., Smith, G.A., Nichols, P.D., White, D.C. & Sullivan, C.W. 1988. Changes in photosynthetic carbon assimilation in Antarctic sea-ice diatoms during spring bloom: variation in synthesis of lipid classes. *J. Exp. Mar. Biol. Ecol.*, 116:1-13.

Peperzak, L. & Brussaard, C. P. 2011. Flow cytometric applicability of fluorescent vitality probes on phytoplankton. *J. Phycol*. 47:692–702.

Peters, E. 1996. Prolonged darkness and diatom mortality: ii. Marine temperate species. *J. Exp. Mar. Biol. Ecol*. 207:43–58.

This article is protected by copyright. All rights reserved

Peters, E. & Thomas, D. N. 1996. Prolonged darkness and diatom mortality i: Marine Antarctic species. *J. Exp. Mar. Biol. Ecol.* 207:25–41.

Poulin, M., Daugbjerg, N., Gradinger, R., Ilyash, L., Ratkova, T. & von Quillfeldt, C. H. 2011. The pan-Arctic biodiversity of marine pelagic and sea-ice unicellular eukaryotes: a first-attempt assessment. *Mar. Biodivers*. 41:13–28.

Price, N. M., Harrison, G. I., Hering, J. G., Hudson, R. J., Nirel, P. M., Palenik, B. & Morel, F. M. 1989. Preparation and chemistry of the artificial algal culture medium Aquil. *Biol. Oceanogr.* 6: 443-61.

R Core Team. 2021. R: A language and environment for statistical computing. R Foundation for Statistical Computing, Vienna, Austria. URL https://www.R-project.org/.

Ras, J., Claustre, H. & Uitz, J. 2008. Spatial variability of phytoplankton pigment distributions in the Subtropical South Pacific Ocean: comparison between in situ and predicted data. *Biogeosci*. 5:353–69.

Remmers, I. M., D'Adamo, S., Martens, D. E., de Vos, R. C. H., Mumm, R., America, A. H. P., Cordewener, J. H. G., Linda V., Bakker, L. V., Peters, S. A., Wijffels, R. H. & Lamers, P. P. 2018. Orchestration of transcriptome, proteome and metabolome in the diatom *Phaeodactylum tricornutum* during nitrogen limitation. *Algal Res.* 35:33–49.

Reeves, S., McMinn, A. & Martin, A. 2011. The effect of prolonged darkness on the growth, recovery and survival of Antarctic sea ice diatoms. *Polar Biol*. 34:1019–32.

Richmond, T. J. & Davey, C. A. 2003. The structure of DNA in the nucleosome core. *Nature* 423:145.

This article is protected by copyright. All rights reserved

Rumin, J., Bonnefond, H., Saint-Jean, B., Rouxel, C., Sciandra, A., Bernard, O., Cadoret, J.P. & Bougaran, G. 2015. The use of fluorescent Nile Red and BODIPY for lipid measurement in microalgae. *Biotechnol. Biofuels* 8:42.

Sakshaug, E. 2004 Primary and Secondary Production in the Arctic Seas. *In* Stein, R. & MacDonald, R. W. [Eds.] *The Organic Carbon Cycle in the Arctic Ocean*. Springer, Berlin, Heidelberg. pp. 57–81.

Schaub, I., Wagner H., Graeve, M. & Karsten, U. 2017. Effects of prolonged darkness and temperature on the lipid metabolism in the benthic diatom *Navicula perminuta* from the Arctic Adventfjorden, Svalbard. *Polar Biol*. 40:1425–39.

Scrucca, L., Fop, M., Murphy, T. B. & Raftery, A. E. 2016. mclust 5: clustering, classification and density estimation using gaussian finite mixture models. *R J*. 8:289.

Talbert, P. B., Meers, M. P. & Henikoff, S. 2019. Old cogs, new tricks: the evolution of gene expression in a chromatin context. *Nat. Rev. Genet*. 20:283.

Tillmann, U., Baumann, M.E. & Aletsee, L. 1989. Distribution of carbon among photosynthetic end products in the bloom-forming arctic diatom *Thalassiosira antarctica* COMBER. *Polar Biol.* 10:231-8.

Thomas, D.N. & Gleitz, M. 1993. Allocation of photoassimilated carbon into major algal metabolite fractions: variation between two diatom species isolated from the Weddell Sea (Antarctica). *Polar Biol.* 13:281-6.

van Tol, H. M., Amin, S. A. & Armbrust, E. V. 2017. Ubiquitous marine bacterium inhibits diatom cell division. *ISME J*. 11:31.

This article is protected by copyright. All rights reserved

Traller, J. C., Cokus, S. J., Lopez, D. A., Gaidarenko, O., Smith, S. R., McCrow, J. P., Gallaher, S. D., Podell, S., Thompson, M., Cook, O., Morselli, M., Jaroszewicz, A., Allen, E. E., Allen, A. E., Merchant, S. S., Pellegrini, M. & Hildebrand, M. 2016. Genome and methylome of the oleaginous diatom *Cyclotella cryptica* reveal genetic flexibility toward a high lipid phenotype. *Biotechnol. Biofuels* 9:1-20.

Veuger, B. & van Oevelen, D. 2011. Long-term pigment dynamics and diatom survival in dark sediment. *Limnol. Oceanogr.* 56:1065–74.

Villanova, V., Fortunato, A. E., Singh, D., Dal Bo, D., Conte, M., Obata, T., Jouhet, J., Fernie, A. R., Marechal, E., Falciatore, A., Pagliardini, J., Le Monnier, A., Poolman, M., Curien, G., Petroutsos, D. & Finazzi, G. 2017. Investigating mixotrophic metabolism in the model diatom *Phaeodactylum tricornutum*. *Philos. T. Roy. Soc. B.* 372:20160404.

Von Quillfeldt, C. H. 2000. Common diatom species in Arctic spring blooms: their distribution and abundance. *Bot. Mar*. 43:499–516.

Walter, B., Peters, J. & van Beusekom, J. E. 2017. The effect of constant darkness and short light periods on the survival and physiological fitness of two phytoplankton species and their growth potential after re-illumination. *Aquat. Ecol*. 51:591–603.

Wulff, A., Roleda, M. Y., Zacher, K. & Wiencke, C. 2008. UV radiation effects on pigments, photosynthetic efficiency and DNA of an Antarctic marine benthic diatom community. *Aquat. Biol*. 3:167–77.

Yang, R. & Wei, D. 2020. Improving fucoxanthin production in mixotrophic culture of marine diatom *Phaeodactylum tricornutum* by LED Light shift and nitrogen supplementation. *Front. Bioeng. Biotechnol.* 8:820.

This article is protected by copyright. All rights reserved

Table 1. Average viability, survival rate and growth parameters upon re-illumination. Each point is the mean of technical replicates of the three biological replicates (n = 9) ± standard deviation.

Survival and growth indexes	1 month	3 months	5 months
Viability (%) at T0	99.03	99.16	97.93
Viability (%) cells before RL[a]	98.5 ± 0.35	98.6 ± 0.40	50.0 ± 0.50
Viability decrease (%) during RL[b]	2.21 ± 2.93	28.33 ± 3.78	46.9 ± 4.50
Days before first increase of the concentration[c]	0.80	5	7
Growth rate (d^{-1})[d]	0.31 ± 0.00	0.31 ± 0.02	0.27 ± 0.12

[a] Viability at $T0_{RL}$, just before the light system was turned back on.

[b] Viability difference between $T0_{RL}$ and the lowest value recorded during RL.

[c] Time of RL at which the first increase of viable cells concentration was recorded.

[d] Calculated by linear regression on natural logarithm transformed concentration of viable cells data corresponding to the exponential growth phase (i.e., linear part of log transformed concentrations curve).

This article is protected by copyright. All rights reserved

Figure 1: Mean BODIPY green fluorescence (neutral lipids; solid line) and carbon quota (dashed line) during the 3-month DA. Each point is the mean of technical replicates of the three biological replicates (n = 9) with their standard deviation as the error bars. Neutral lipid content is expressed as relative units (r.u.).

Figure 2: Density scatter plot showing P1, P2 and P3 after three months of darkness. (A) Plotting the red fluorescence as a function of the forward scatter allows to distinguish P2 from P1 and P3. (B) Plotting the SYBR Green data as a function of the side scatter allows to distinguish P3 from P1 and P2. The procedure used to statistically confirm the existence of three distinct populations as they are defined here is detailed in Appendix S1 in the Supporting Information. Relative units (r.u.).

Figure 3: Mean cell concentrations during 3-month DA and subsequent RL. The first panel shows that the growth of P2 and P3 and the decrease observed in P1 are concomitant and of similar magnitude during DA. P2 and total cell concentrations were estimated in flow cytometry samples without addition of dye. Each point is the mean of technical replicates of the three biological replicates (n = 9). Cells belonging to P1 and P3 could only be distinguished from each other in SYBR Green samples in which the number of cells detected may vary slightly with staining efficiency. Therefore, for each sampling time and each culture, P1 and P3 concentrations were first estimated in the SYBR Green samples before the concentrations were corrected by being multiplied by the ratio of (P1+P3) concentrations measured in SYBR Green and samples without dye. For these two populations, each point is the mean of the three biological replicates (n = 3) as only one technical replicate was made for SYBR Green. Error bars represent the standard deviation.

Figure 4: Mean forward scatter and red fluorescence during the 3-month DA and subsequent RL. Data for P2 and P3 were only plotted from the day they represented at least 1 % of the total cell concentration (i.e., day 31 and 36 of the DA, respectively). SYBR Green samples have been used to retrieve data of P1 and P3 which could only be distinguished in these samples. The red fluorescence was not affected by staining with SYBR Green. The average of the ratio of the values obtained for samples with SYBR Green and without die was of 1.00 ± 0.04. FSC was, on the other hand,

This article is protected by copyright. All rights reserved

Accepted Article

systematically underestimated by approximately 17% in SYBR Green samples (ratio: 0.83 ± 0.02). For each of the two parameters, values retrieved from the SYBR Green data have been corrected by being divided by the corresponding average ratio. Each point is the average of three biological replicates (n = 3) with their standard deviation as the error bars. Because P2 was characterized by a very low SYBR Green fluorescence, some cells were below the threshold set in the protocol and were not detected. Therefore, data for P2 were retrieved from the samples without die. Each point is the mean of three technical replicates of the three biological replicates (n = 9) with their standard deviation as the error bars. Forward scatter and red fluorescence are expressed as relative units (r.u.).

Figure 5: Mean SYBR Green fluorescence of P1 and P3 during the 3-month DA and subsequent RL. Because some cells of P2 were characterized by a very low SYBR Green fluorescence, they were below the threshold and not detected. Data for P2 are therefore not available. Each point is the mean of the biological replicates (n = 3). SYBR Green fluorescence is expressed as relative units (r.u.).

Figure 6: BODIPY fluorescence of P2. Relative units (r.u.). (A) Cytogram showing the pattern of BODIPY green fluorescence of P1 and P2 at the end of DA after staining with BODIPY. (B) BODIPY fluorescence for P2 during the 3-month DA and subsequent RL. Data have been plotted after P2 had grown enough to represent more than 1 % of the total cell concentration (i.e., day 31). Each point is the mean of the technical replicates of all biological replicates (n = 9) with their standard deviation as the error bars. Vertical bars represent the standard deviation.

Figure S1: Light spectrum in the cylinders. The integral of the curve equals 30 µmol photons m^{-2} s^{-1}. The light intensity was measured with a radiometer USB-4000 (Ocean Insight) every 21 nm. The light probe was placed in the middle of the cylinders.

Figure S2: Example of cytograms showing (A) the cell concentration, the red fluorescence and the FSC, (B) the neutral lipids content, (C) the viability, (D) the genetic material fluorescence and to detect the eventual presence of contaminant organisms. Relative units (r.u.).

This article is protected by copyright. All rights reserved

Figure S3: Viability of cultures for each of the three DA before RL estimated with SYTOX Green (i.e., membrane permeability test). Each point is the mean of the technical replicates of all biological replicates (n = 9) with their standard deviation as the error bars.

Figure S4: Appearance of the P2 population (red) next to the P1 population (green) during DA. The four panels are cytograms selected from all those available and deemed relevant to visually illustrate P2 appearance during DA. Cal. beads = calibration beads. Relative units (r.u.).

Figure S5: Size distribution curves of the three cultures of *Fragilariopsis cylindrus* after three months of darkness estimated on the Multisizer 4. For each of the three biological replicates, cell numbers in 12.5 µl are given for each size bean (0.16 µm) between 2.5 and 6 µm. Each point is the mean of three technical replicates (n = 3).

Figure S6: Linear regression between the FSC and red fluorescence and green fluorescence values of the population containing P1 and P3 showing the dependency of FSC estimations on chl *a* and NL contents in darkness for the 3-month DA cultures. Each point is the mean of the technical replicates for each biological replicate (n = 3). Relative units (r.u.).

Figure S7: Viability of P1 et 2 stained with SYTOX Green (A) after 3-month DA and (B) after five days of re-illumination. During DA, the majority of P2 was not stained and cells were viable according to the protocol. However, the same cells were also not stained by SYTOX Green during RL, although they underwent significant degradation of their contents after re-exposure to light. Relative units (r.u.).

Figure S8: DNA stained with SYBR Green fluorescence pattern of P2. P1 and P3 cells have been removed to better see P2 cells distribution. Because the noise represented an extremely dense cloud of particles, a detection threshold was set on the green fluorescence in order to detect enough *Fragilariopsis cylindrus* cells. Because of this, the P2 population could not be detected in its entirety as some of its cells were characterized by very low SYBR Green fluorescence. Relative units (r.u.).

This article is protected by copyright. All rights reserved

Figure S9: Decrease of the FSC and red fluorescence of P2 cells during RL. The four panels are cytograms selected from all those available and deemed relevant to visually illustrate P2 degradation during RL. Cal. beads = calibration beads. Relative units (r.u.).

Figure S10: Appearance and development of the P3 population (blue) during DA. The SYBR Green fluorescence of P1 first decreases during the first weeks. After approximately 50 days, cells with very high SYBR Green fluorescence start to appear over P1 and continue to accumulate afterward to form P3. Cells belonging to P2, identified via FSC and red fluorescence values, are also distinguishable from the two other populations and are characterized by a lower SYBR Green fluorescence similar to that of the background noise. The four panels are cytograms selected from all those available and deemed relevant to visually illustrate P3 appearance during DA. Cal. beads = calibration beads. Relative units (r.u.).

Figure S11: Cytogram showing no differences between P1 and 3 in terms of FSC and red fluorescence at day 87 of DA. Relative units (r.u.).

Figure S12: Cytograms showing P3 red fluorescence and FSC decreasing 24 h after RL, rejoining progressively the P2 population. Relative units (r.u.).

Figure S13: Degradation of the P3 population (blue) during RL. While the red fluorescence of P1 began to increase 8 hours after the start of RL, the red fluorescence of P3 never stopped decreasing. On the third day, the green SYBR fluorescence of P1 had already increased significantly while that of P3 remained unchanged. The cell concentration of the P3 population decreased, whereas the P2 population increased significantly. It is also evident here that P2 cells, losing their red fluorescence, are lost in the background noise, probably composed of the remains of dead cells. Note that only 5,000 events instead of 2,0000 were counted 24 h after RL. The four panels are cytograms selected from all those available and deemed relevant to visually illustrate P3 degradation during DA. Cal. beads = calibration beads. Relative units (r.u.).

Figure S14: Average cell pigment contents during the 3-month DA. A. Chlorophyll *a* (solid line) and fucoxanthin (dashed line). B. β-carotenes. C. Diadinoxanthin (solid line) and Chlorophyll *c*

This article is protected by copyright. All rights reserved

(dashed line). Each point is the mean of the three biological replicates (n = 3) with their standard deviation as the error bars.

Table S1: Preparation of cultures: *Fragilariopsis cylindrus* growth conditions before the start of the experiments. Prior to experiments, *F. cylindrus* cells were maintained in stable semi-continuous culture conditions and cultivated in incremental volumes to reach a final volume of 80 L of acclimated culture in each cylinder.

Table S2: Sampling timeline for each of the two experiment phases of the three DA. For RL, the sampling times mentioned are the times since re-illumination. In each experiment, the light system was started 24 h after the last sampling time of DA.

Accepted Article

This article is protected by copyright. All rights reserved

Accepted Article

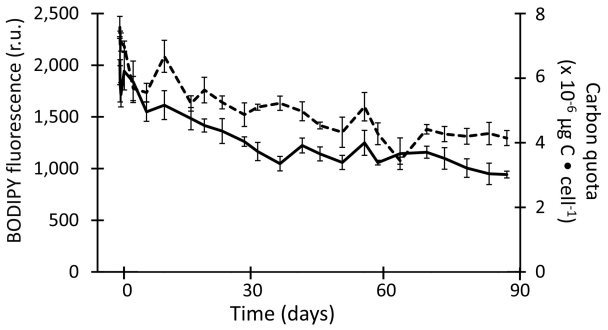

jpy_13232_f1.tif

This article is protected by copyright. All rights reserved

Accepted Article

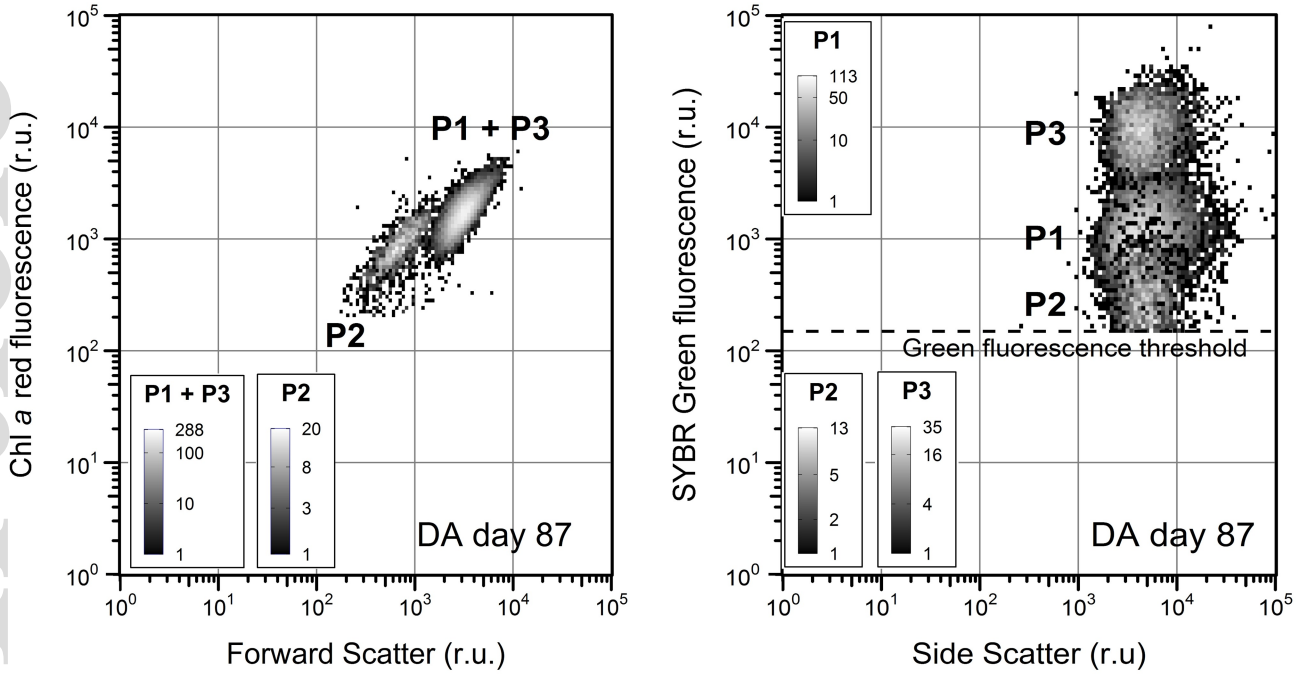

jpy_13232_f2.tif

This article is protected by copyright. All rights reserved

Accepted Article

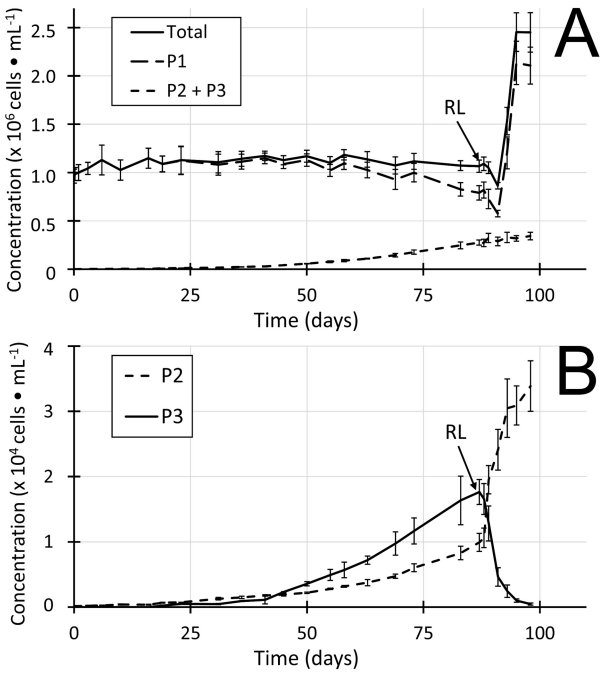

jpy_13232_f3.tif

This article is protected by copyright. All rights reserved

Accepted Article

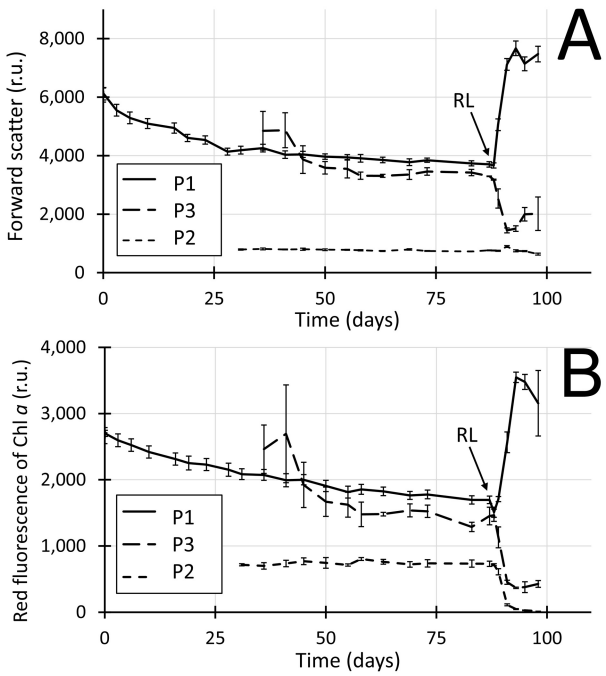

jpy_13232_f4.tif

This article is protected by copyright. All rights reserved

Accepted Article

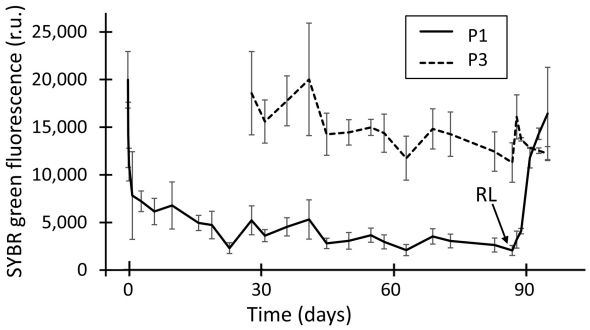

jpy_13232_f5.tif

This article is protected by copyright. All rights reserved

Accepted Article

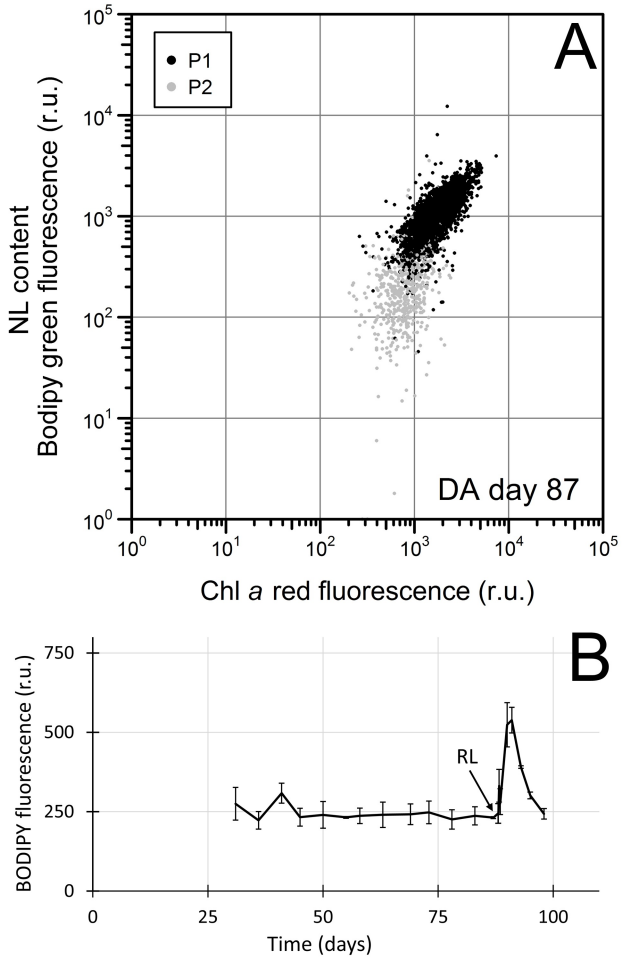

jpy_13232_f6.tif

This article is protected by copyright. All rights reserved